Identifying inhibitors of epithelial-mesenchymal plasticity using a network topology based approach

Kishore Hari[1], Burhanuddin Sabuwala[2], Balaram Vishnu Subramani[3], Caterina La Porta[4,5], Stefano Zapperi4[4,6], Francesc Font-Clos[4,6], Mohit Kumar Jolly[1*]

[1] Centre for BioSystems Science and Engineering, Indian Institute of Science, Bangalore 560012, India

[2] Department of Biotechnology, Indian Institute of Technology Madras, Chennai 600036, India

[3] School of Mathematics, Indian Institute of Science Education and Research, Thiruvananthapuram 695551, India

[4] Center for Complexity and Biosystems, University of Milan, Milano 20133, Italy

[5] Department of Environmental Science and Policy, University of Milan, Milano 20133, Italy

[6] Department of Physics, University of Milan, Milano 20133, Italy

[*] Corresponding author: mkjolly@iisc.ac.in

Abstract

Metastasis is the cause of over 90% of cancer-related deaths. Cancer cells undergoing metastasis can switch dynamically between different phenotypes, enabling them to adapt to harsh challenges such as overcoming anoikis and evading immune response. This ability, known as phenotypic plasticity, is crucial for the survival of cancer cells during metastasis, as well as acquiring therapy resistance. Various biochemical networks have been identified to contribute to phenotypic plasticity, but how plasticity emerges from the dynamics of these networks remains elusive. Here, we investigated the dynamics of various regulatory networks implicated in Epithelial-Mesenchymal Plasticity (EMP) − an important arm of phenotypic plasticity − through two different mathematical modelling frameworks: a discrete, parameter-independent framework (Boolean) and a continuous, parameter-agnostic modelling framework (RACIPE). Results from either framework in terms of phenotypic distributions obtained from a given EMP network are qualitatively similar and suggest that these networks are multi-stable and can give rise to phenotypic plasticity. Neither method requires specific kinetic parameters, thus our results emphasize that EMP can emerge through these networks over a wide range of parameter sets, elucidating the importance of network topology in enabling phenotypic plasticity. Furthermore, we show that the ability to exhibit phenotypic plasticity positively correlates with the number of positive feedback loops. These results pave a way towards an unorthodox network topology-based approach to identify crucial links in a given EMP network that can reduce phenotypic plasticity and possibly inhibit metastasis - by reducing the number of positive feedback loops.

Keywords: *Epithelial-Mesenchymal Plasticity (EMP), bidirectional transition, network topology, RACIPE, Boolean models, parameter independent and parameter agnostic models*

1. Introduction

Metastasis, therapy resistance, and tumor relapse remain unsolved clinical challenges and a major cause of cancer mortality [1]. During metastasis, cells navigate many bottlenecks: local invasion, intravasation, survival in circulation in matrix-deprived conditions, extravasation, and eventually colonization of the distant organ. Only a few ($< 0.02\%$) cells survive this cascade of events and are capable of initiating metastasis. Recent studies have identified phenotypic plasticity − the ability of cells to reversibly switch phenotypes in response to their ever-changing environmental conditions − as a hallmark of cancer metastasis [2]. Similarly, phenotypic plasticity enables a small proportion of cancers cells to transiently acquire an adaptive drug-refractory phenotype which may contribute to tumor relapse [3]. Therefore, identifying the mechanisms of phenotypic plasticity is essential for any major breakthroughs in cancer treatment.

Phenotypic plasticity is considered to be an adaptation strategy to survive in variable environmental conditions [4]. Recently, the contributions of phenotypic plasticity in driving metastasis and therapy resistance have been realized more prominently, especially due to the lack of any unique mutational signature being identified for cancer metastasis so far [2], and the frequent emergence of resistance against targeted therapy [3]. Phenotypic plasticity, referred to as "the architect who never sleeps" [5], can have various dimensions – metabolic plasticity [6], epithelial-mesenchymal plasticity [7], plasticity between cancer stem cell (CSC) and a non-CSC state [8, 9, 10], and plasticity between drug-sensitive and drug-resistant/tolerant state [11] among others. Cancer cells continually exploit phenotypic plasticity to adapt to their ever-changing environment by maximizing their fitness during cancer progression, metastasis, therapy resistance and eventually tumor relapse [12]. Moreover, phenotypic plasticity can amplify the non-genetic heterogeneity within tumors, thus increasing the number of 'exit options' for cells in response to drugs, thereby increasing the versatility of the tumor cell population [13]. Thus, targeting phenotypic plasticity provides a unique opportunity to both curb cancer metastasis and to improve the efficiency of existing therapeutic strategies.

A canonical example of phenotypic plasticity is Epithelial-Mesenchymal plasticity (EMP), which involves partial and/or complete Epithelial-Mesenchymal Transition (EMT) and/or Mesenchymal-Epithelial Transition (MET). EMT and MET are embryonic developmental programs which are often adopted by cancer cells during metastasis [14]. EMT can fuel the dissemination of stationary cancer cells through reduced cell-cell adhesion and apico-basal polarity and increased migration and invasion. Conversely, MET may enable the disseminated cells that exit the bloodstream to survive in a different environment by regaining cell-cell adhesion and proliferation to eventually colonize that

3

organ. EMT and MET were earlier thought of as binary processes (i.e. switching between epithelial and mesenchymal phenotypes), but recent *in vitro*, *in vivo* and *in silico* evidence strongly suggests that they are not 'all-or-none' processes, and cells can stably reside in one or more hybrid E/M phenotypes, thus enabling various manifestations of EMP [14]. EMP can not only drive metastasis, but also influence the resistance to various chemotherapeutic drugs and targeted therapies. It can also alter the tumor microenvironment to be immunosuppressive, eventually leading to overall poor survival of patients across cancer types [15, 16]. Therefore, preventing the ability of cells to reversibly switch among these epithelial (E), mesenchymal (M), and hybrid E/M (H) phenotypes can have a significant clinical impact.

Most current preclinical and clinical efforts attempt to restrict EMP in only one direction – EMT or MET. Such efforts are likely to facilitate the transition in the opposite direction (i.e. MET or EMT respectively) and can possibly increase the frequency of hybrid E/M phenotypes which can be the 'fittest' for metastasis [17]. Hence, these interventions may increase the metastatic load instead, depending on the phenotypic distribution of disseminated cells. Blocking EMP in both directions can overcome these potential side effects. Moreover, restricting EMP bidirectionally can also limit the ability of a clonal population to generate and/or maintain non-genetic heterogeneity [18]. Non-genetic heterogeneity can enable 'bet-hedging' during the evolution of drug resistance [19], as well as the co-existence of phenotypically distinct subpopulations of epithelial and mesenchymal cells that can communicate and cooperate among themselves to aggravate metastasis [20, 21]. Thus, blocking EMP bidirectionally, or in other words "fixing cells at a given position on the epithelial-–mesenchymal axis to prevent access to the range of states that might be required to facilitate different stages of the metastatic cascade" [22], is likely to blunt the metastatic and drug-resistance potential of cancer cells much stronger than restricting only EMT or only MET.

Identifying ways to inhibit EMP requires a detailed mechanistic understanding of its dynamics. Experimentally, EMP can be tracked through recent advances such as live-cell imaging reporter constructs or single-cell RNA-seq and/or mass/flow cytometry [13]. Another approach to characterize the dynamics of EMP is by developing mechanism-based mathematical models of networks that have experimentally been identified to regulate EMT and/or MET. Many such mathematical models have helped gain useful insights into the dynamics of EMP and have driven the experiments to decode a) how cells attain one or more hybrid E/M phenotype, b) how reversible is EMP in both directions (E to M vs. M to E) and c) whether cells take same or different paths en route EMT or MET [23]. However, none of these models investigated the possibility of identifying mechanisms to block EMP

65 bidirectionally.

66   Here, we investigate the dynamics of various regulatory networks implicated in EMP and identify

67 robust network topology based design principles of EMP, using two different but complementary

68 modeling formalisms – a discrete , parameter-independent method: asynchronous Boolean [24] and a

69 continuous, parameter-agnostic method: RACIPE (Random Circuit Perturbation) [25]. Our results

70 show that the phenotypic distributions that can be obtained through an EMP network depend

71 majorly on network topology but are largely independent of specific kinetic parameters for each link

72 in the network. We also pinpoint a set of network perturbations that can reduce EMP, and observe a

73 unifying theme amongst them: a reduced number of total positive feedback loops embedded within

74 an EMP network led to curtailed EMP. Therefore, our approach unravels the common operating

75 principles of various EMP regulatory networks and offers a systematic framework to identify network

76 perturbations to restrict EMP based on this network topology-based dynamical trait.

2. Results

2.1. RACIPE and Boolean models have similar phenotypic distributions for EMP networks

79   Boolean frameworks lack kinetic parameters and treat a gene to be discretely ON (1) or OFF

80 (0), thus focusing on a coarse-grained view of how various interactions in a network can give rise

81 to the repertoire of dynamical behaviours [26]. RACIPE, on the other hand, generates an ensemble

82 of continuous mathematical models (sets of coupled ordinary differential equations) with randomly

83 chosen kinetic parameters for a given network topology and clusters the steady state solutions to

84 identify the robust dynamical features of a given network. In other words, while a Boolean framework

85 is parameter-independent, RACIPE can be thought of as a parameter-agnostic one.

86   Therefore, the similarity in dynamical traits of a network simulated via Boolean and RACIPE

87 frameworks can unravel the extent to which the network topology drives the network dynamics,

88 without much reliance on the specific choice of kinetic parameters. Across various EMP networks

89 and the perturbations made in those, we have compared the outputs of these two modeling frameworks

90 in terms of phenotypic distributions, and in ranking the effect of various perturbations in diminishing

91 EMP (**Fig 1A**).

92   We have investigated 6 different networks reported in EMP literature; these networks vary from 3

93 nodes to 8 nodes and 7 edges to 16 edges (**Fig 1B**). First, we calculated the phenotypic distributions

94 (i.e. stable steady state frequency distributions) obtained via RACIPE and Boolean models. To

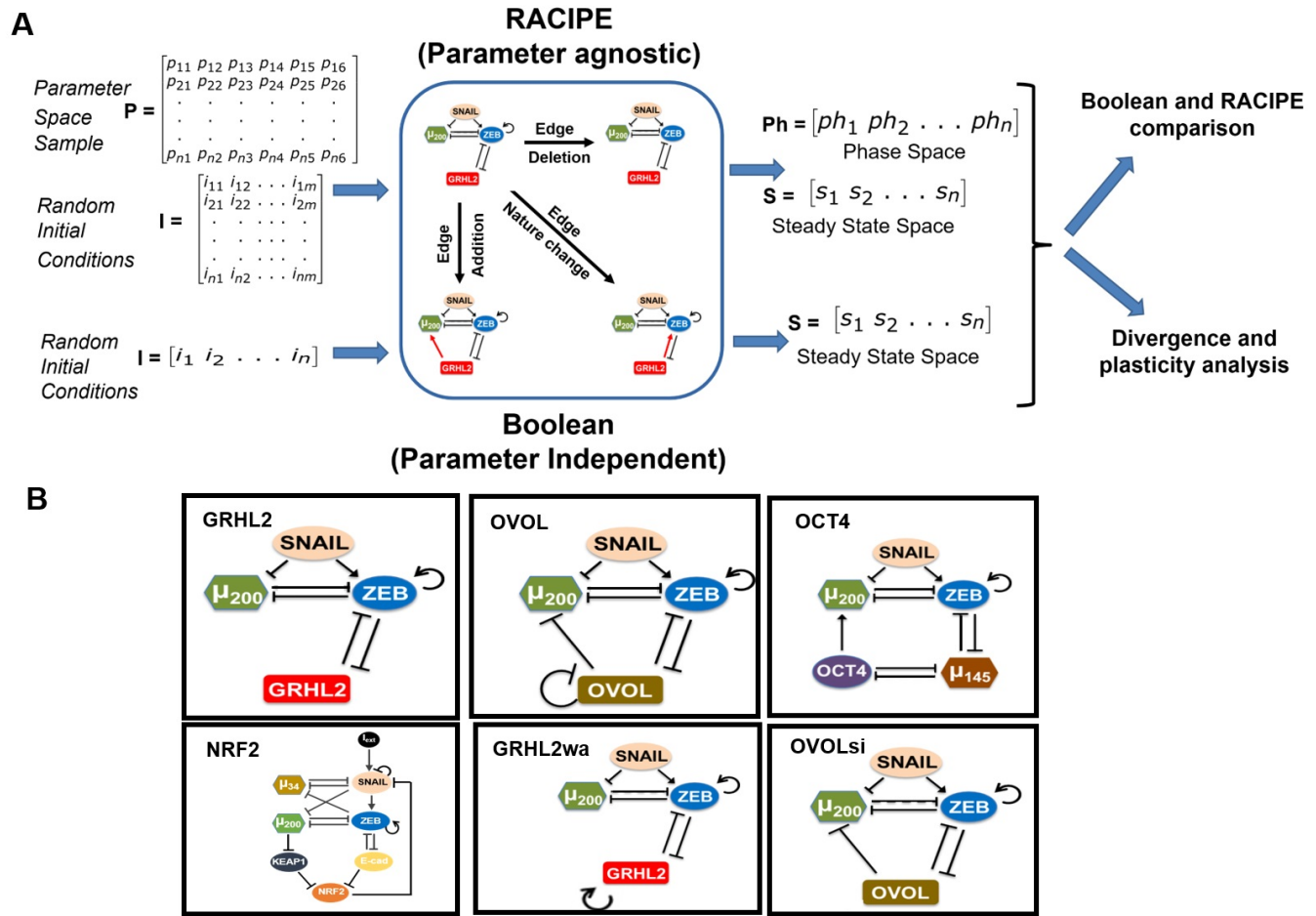95 facilitate the comparison of Boolean and RACIPE models, we have discretized the output of RACIPE

5

Figure 1: Dynamical approaches to investigate EMP. A. Schematic of network analysis strategy. For a given EMP network, both the 'wild type'and perturbed networks are simulated via both RACIPE and Boolean. The steady state and phase frequency distributions thus obtained are further analysed to elucidate similarities between RACIPE and Boolean as well as identifying the factors underlying phenotypic plasticity. B. EMP networks analysed in the study.

96 (as described in 'Methods' section). First, we determined the sample size of parameter sets to be

97 chosen for RACIPE, and the number of initial conditions for Boolean models, using a quantitative

98 convergence analysis. N=10,000 was chosen as the optimal number of parameter sets for RACIPE,

99 and as the optimal number of initial conditions for Boolean analysis, based on observed standard

100 deviation in steady state distributions obtained from RACIPE and Boolean models (**Fig 2A, S1A**).

101   For the miR-200/ZEB/ SNAIL/GRHL2 network (hereafter called as 'GRHL2 network'; 4 nodes,

102 7 edges), a maximum of $2^3 = 8$ stable steady states are possible (value of each node $= 0$ or 1;

103 SNAIL is an input to the circuit), in discretized RACIPE and Boolean framework. From Boolean

104 analysis, we obtained four stable states for this network across different numbers of initial conditions

105 chosen. Two out of these four states were more prominent − (ZEB=0, miR-200=1, GRHL2=1) and

106 (ZEB=1, miR-200=0, GRHL2=0) − than the others (**Fig 2A, i**). These two states can be construed

107 as epithelial (high miR-200 and GRHL2, low ZEB) and mesenchymal (low miR-200 and GRHL2,

108 high ZEB) phenotypes as observed experimentally [27]; [28]. Discretized analysis of RACIPE results

109 also identifies the four stable steady states and with similar relative frequency as seen in the case of

110 Boolean model and 3 other states with relatively less frequencies (**Fig 2A, ii**). Put together, these

111 results suggest that epithelial and mesenchymal phenotypes are the two most commonly expected

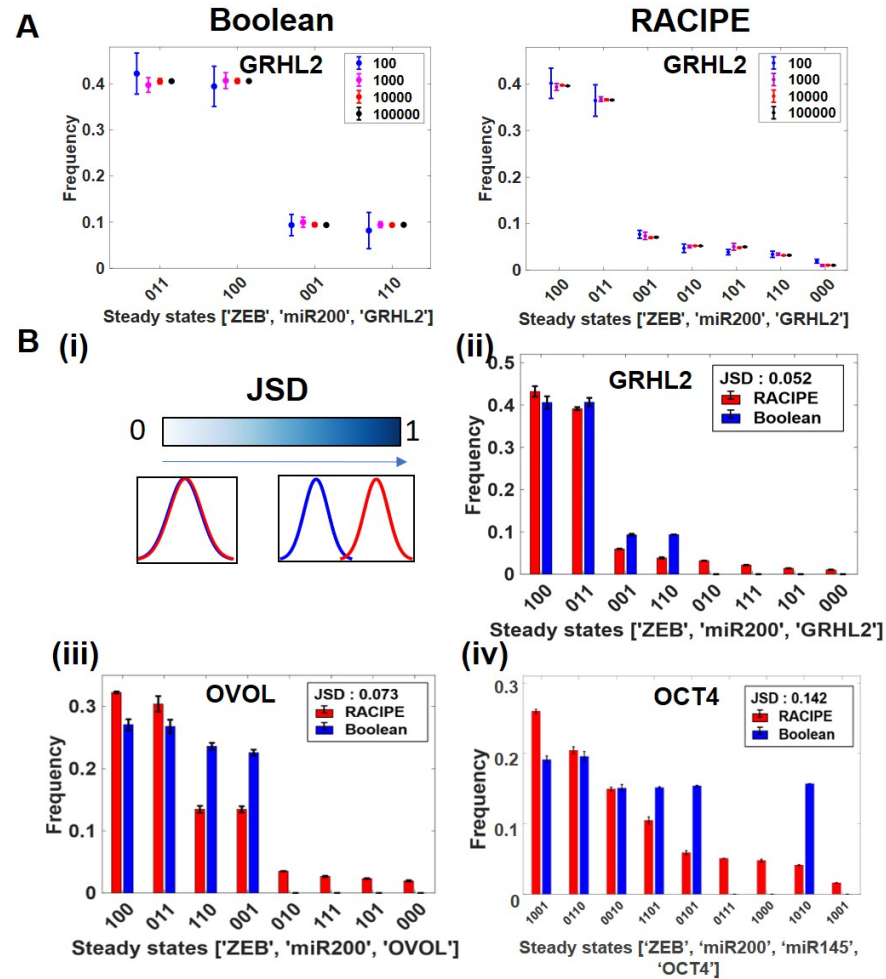112 phenotypes from the dynamics of GRHL2 network.

Figure 2: Comparing the outcomes of the discrete (Boolean) and the continuous (RACIPE) modelling frameworks A. Quantitative convergence (QC) of the state frequency landscape for different number of initial conditions in Boolean analysis (i) and different number of parameter sets randomly sampled from the parameter space for RACIPE (ii) respectively. Error bars represent the mean SD of the corresponding frequencies obtained by n = 3 independent simulations. B. i) Demonstration of JSD between two given probability distributions; JSD ranges from 0 to 1. ii)-iv) Comparison of phenotypic frequency distributions for different EMP networks, as obtained from Boolean and RACIPE.

113 GRHL2 and OVOL1/2 are reported to play similar roles in inducing MET and/or inhibiting

114 EMT [29, 30, 31]. Thus, epithelial (ZEB=0, miR-200=1, OVOL=1) and mesenchymal (ZEB=1,

miR-200=0, OVOL=0) phenotypes are seen consistently as most predominant ones in the RACIPE and Boolean model results for the SNAIL/miR-200/ZEB/OVOL network as well (**Fig S1A, i**). Since GRHL2 can self-activate [32] and OVOL can self-inhibit[33], we studied networks with GRHL2 self activation (referred to as GRHL2wa) and with and without OVOL self-inhibition (OVOL and OVOLsi respectively) (**Fig 1B**). In both Boolean and RACIPE, we observed that epithelial and mesenchymal states were the highest frequency phenotypes across these 3 cases(**Fig S1A, iii-iv**).

For the SNAIL/miR-200/ZEB/OCT4/miR-145 network (hereafter referred to as 'OCT4' network; 5 nodes, 10 edges), a maximum of $2^4 = 16$ stable steady states are possible (value of each node = 0 or 1; SNAIL is an input to the circuit). Boolean analysis across different numbers of initial conditions identified six out of the 16 possible states as stable steady states. The most predominant phenotypes were (ZEB=0, miR-200=1, miR-145=0, OCT4=0) and (ZEB=1, miR-200=0, miR-145=1, OCT4=1) which can be mapped on to epithelial and mesenchymal states correspondingly. Results obtained via RACIPE analysis are qualitatively consistent with those from Boolean model; with some additional but less frequent states identified via RACIPE (**Fig S1A, ii**). Similar consistency is observed when comparing the phenotypic distributions for SNAIL/miR-200/ZEB/miR-34/NRF2/KEAP1 network (hereafter called as 'NRF2 network'; **Fig S1C**)

Next, for each of these different EMP networks, we quantified the difference between the phenotypic distributions obtained via RACIPE and Boolean models, using an information theory metric known as the Jensen-Shannon Divergence (JSD). JSD measures the dissimilarity between two given probability distributions and was calculated such that it varies between 0 and 1 (Lin, 1991); the larger the JSD, the more dissimilar or further apart are the two frequency distributions (**Fig 2B, i**). JSD for Boolean vs. RACIPE solutions for the EMP networks modelled here varies between 0.05 to 0.27 (**Fig 2B; S1B; S1C**), suggesting a good quantitative agreement between the two methods. Thus, these results indicate that the phenotypic distributions enabled by these EMP networks is a feature of the underlying network topology rather than of specific kinetic parameters.

2.2. *Quantifying the effect of edge perturbations on phenotypic distributions of EMP networks via JSD*

To characterize the effects of network topology on phenotypic distributions further, we made changes to the topology in the form of single-edge perturbations and quantified the impact of these edge perturbations on the phenotypic distributions obtained from various EMP networks. An edge perturbation can be one of the following: a) deleting an edge, b) adding a (hypothetical) edge, and

8

146 c) changing the sign of an edge (i.e. from activation to inhibition or vice-versa). For a network with

147 N nodes and E edges, there can be E edge deletions, ($^{N}C_2 - E$) additions, and E changes in edge

148 sign. Thus, for the 'wild-type' (WT) SNAIL/miR-200/ZEB/GRHL2 network, 31 such perturbations

149 are possible (**Table S1**), each of which will generate a new network topology. For every pertur-

150 bation, we simulated the new network using both RACIPE and Boolean models and obtained the

151 two corresponding phenotypic distributions. For the 32 distributions (31 perturbed + 1 'wild-type')

152 obtained via Boolean models, we then calculated the JSD between every two phenotypic distributions

153 to identify perturbations that can drastically alter the phenotypic landscape. The network where the

154 link from ZEB to GRHL2 was changed from inhibtion to activation/excitation (*ZEB-GRHL2_2-1*)

155 had the highest JSD from all remaining 31 networks (**Fig 3A**). RACIPE models, in addition to

156 *ZEB-GRHL2_2-1* identified another perturbation which stood out relative to others – the deletion of

157 the inhibitory link from ZEB to miR-200 (*Zeb-miR200_2-0*) (**Fig 3B**). Similar analysis for the NRF2

158 network using Boolean analysis identified two key perturbations while RACIPE analysis identified

159 two additional ones (**Fig S2A**).

160 Further, we compared JSD between perturbed and 'wild-type' networks, calculated via RACIPE

161 and Boolean analysis (**Fig 3C, S2B**). While the absolute values of JSD were different for Boolean

162 and RACIPE methods, a positive correlation was observed between the JSD values across all six

163 EMP networks considered here. Moreover, the strongest perturbation obtained via both methods

164 showed concordance (highligled by the arrows in **Fig 3C and S2B**). These results further emphasize

165 the role of network topology in phenotypic distributions generated by EMP networks.

166 *2.3. JSD does not correlate with phenotypic plasticity in EMP networks*

167 Next, we investigated whether the perturbed networks which are farthest from the 'wild-type'

168 network (i.e., having the highest JSD) are the ones with reduced phenotypic plasticity as well.

169 Phenotypic plasticity is the ability of cells to sample multiple phenotypes (stable steady states)

170 and to switch from one phenotype to another, spontaneously or under external factors. Here, we

171 define phenotypic plasticity in two different ways based on RACIPE output. For every randomly

172 chosen parameter set, RACIPE chooses 100 initial conditions and its output includes the possible

173 one or more stable steady states for a given parameter set, depending on initial conditions. For some

174 parameter sets, all chosen initial conditions converge to one stable state, while in others, multiple

175 steady states (multistability) may be allowed. Thus, plasticity score 1 (PS1) is defined as the fraction

176 of parameter sets that enable multistability (**Fig 4A**). The definition of plasticity score 2 (PS2) is
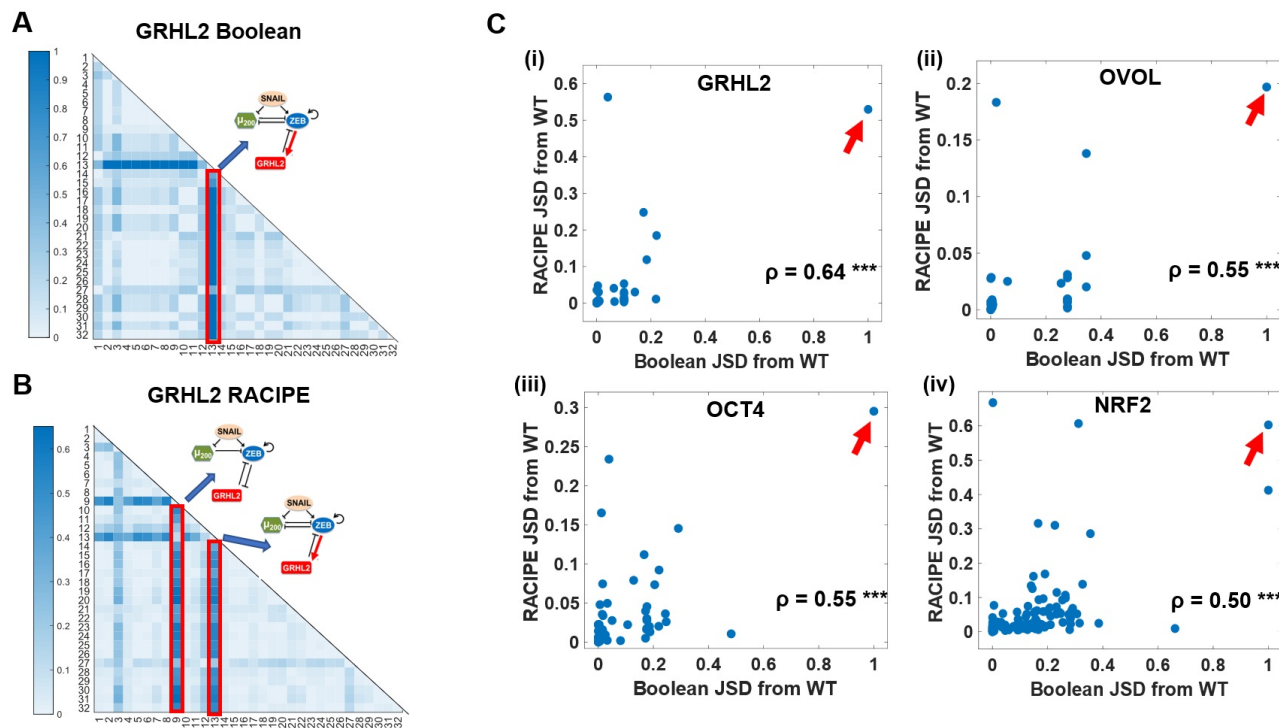
Figure 3: Quantifying the effect of single-edge perturbations on the network behaviour landscapes: A. Heatmap of the distance between steady state distributions of all perturbations for the GRHL2 network from each other, obtained from Boolean. Color bar shows the value of JSD. Each number (1-31) represents a particular perturbed network and number 2 represents 'wild-type' (**Table S1**). The change of ZEB-GRHL2 link from inhibition to activation (highlighted in red) has high JSD from all other perturbations and WT. B. Same as A, but for results via RACIPE. In addition to the one identified via Boolean analysis, this heatmap highlights another perturbed network where the inhibitory link from ZEB to miR-200 is broken. C. Scatter plots of JSD between the steady state distributions of a perturbed network from WT as obtained via RACIPE vs. as obtained via RACIPE. Each dot in a plot represents a perturbed topology for the EMP network mentioned – GRHL2 in i), OVOL in ii), OCT4 in iii) and NRF2 in iv). The strongest perturbation identified by both Boolean and RACIPE is highlighted by the arrow. Spearman correlation coefficients (ρ) are reported; ***: $p < 0.001$

more biology-centric. We first define the 'phenotype' of a given steady state based on the discretized expression levels of canonical epithelial and mesenchymal markers – miR-200 and ZEB respectively. This allows identifying various phases (combinations of co-existing steady states), such as the co-existence of epithelial and mesenchymal states {E,M} for instance. PS2 is the fraction of parameter sets which allow multiple phenotypic states, i.e. multistable phases (**Fig 4A**). For a given network, we calculated PS1 and PS2 scores for the 'wild-type' and perturbed topologies; a comparison of these two metrics revealed a strong positive correlation across all 6 networks (**Fig 4B, S3A**). The perturbed networks had both increasing as well as decreasing effect on phenotypic plasticity (**Fig 4B, S3A**).
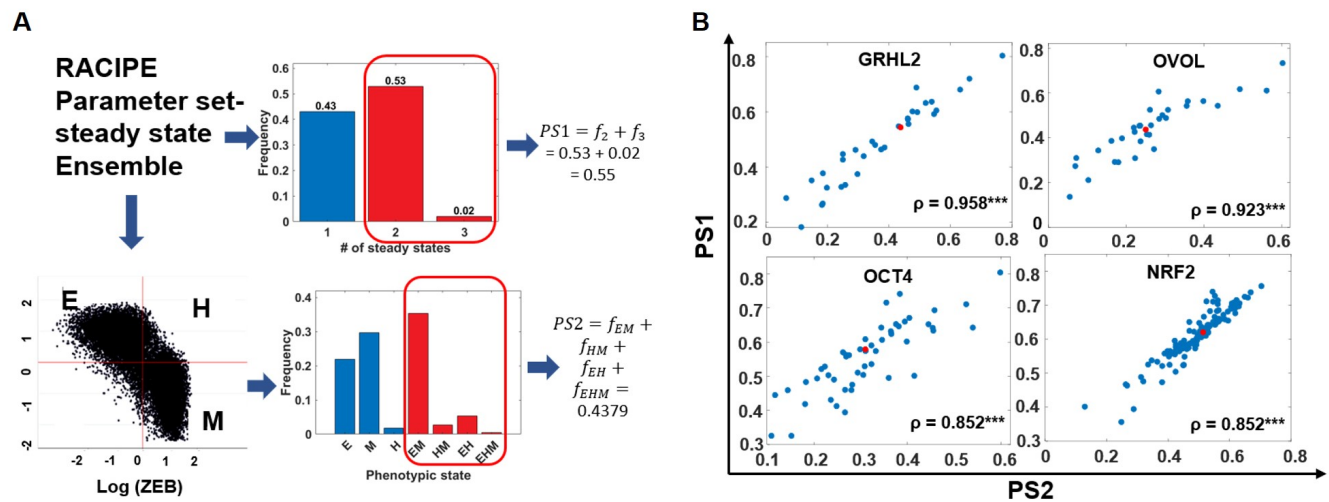
Figure 4: Metrics for quantifying phenotypic plasticity for the case of single-edge perturbations A. Two definitions or plasticity: PS1 (top) is defined as the fraction of multistable parameter sets identified by RACIPE. PS2 (bottom) is calculated after ZEB and miR200 expression levels are used to classify each steady state into Epithelial (E) – (high miR-200, low ZEB) / Hybrid (H) – (high miR-200, high ZEB) / Mesenchymal (M) – (low miR-200, high ZEB) states. Parameter sets are then characterized as monostable or multistable based on the phenotypic states they sample. PS2 is the fraction of parameter sets giving rise to multiple phenotypes. B. Scatter plot of PS1 vs. PS2 for different EMP networks – WT (colored red) and perturbed (colored blue; single-edge perturbed: edge deletion, edge nature change and edge additions) ones. Spearman correlation coefficients (ρ) are denoted; ***: p <0.0001

Further, we checked whether the topologies with the highest JSD from the 'wild-type' network led to a decrease or an increase in PS2 scores. We did not observe any significant overlap of the network topologies with the highest JSD vs. those with the highest or the lowest PS2 scores. This lack of trend was seen across all six networks considered (**Fig 5A**). Further, a scatter plot between JSD from the 'wild-type' network and fold-change in PS2 scores relative to the 'wild-type' was plotted. While some networks showed a negative correlation, others had no significant correlation between these two metrics (**Fig 5B; S3B**) Similar results were obtained for analysis done using PS1 scores for these perturbed networks (**Fig S3C**). Together, these observations suggest that JSD is not a good predictor of phenotypic plasticity.

2.4. Number of positive feedback loops in EMP networks correlates with phenotypic plasticity

Next, we revisited the network topologies with the highest JSD from the 'wild-type' network to identify any topological signatures and observed that all of them were disrupting an overall positive feedback loop in the 'wild-type'. Here, the 'overall' sign of a loop is defined by the product of signs of edges (positive for activation, negative for inhibition) that form a cycle/loop; thus, a mutually
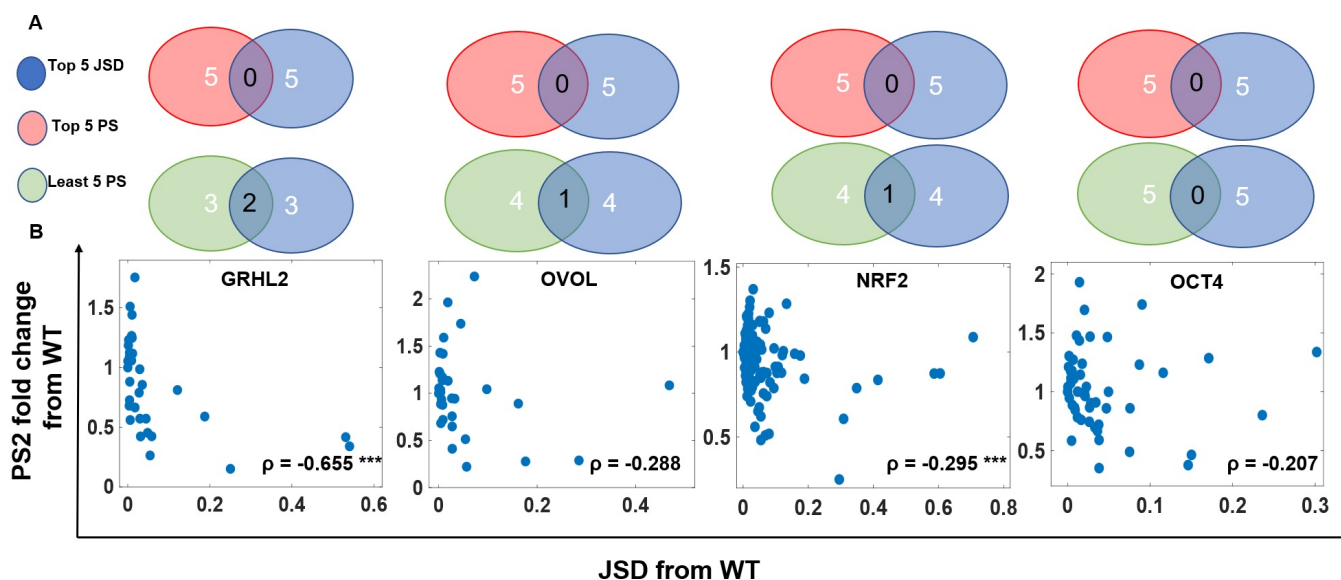
11

Figure 5: JSD does not correlate with phenotypic plasticity. i) Venn diagrams showing the extent of overlap among the perturbed networks that have the highest JSD from the 'wild type' network and those with the highest or lowest fold change in plasticity scores (PS2). EMP networks shown are (from left to right): GRHL2, OVOL, NRF2, OCT4. ii) Scatter plots for respective EMP networks. Each blue dot in a scatter plot is a perturbed network topology corresponding to that EMP network. Spearman correlation coefficient (ρ) are denoted; ***: p<0.001

inhibitory loop between two molecular players is effectively a positive feedback loop. In the GRHL2 network, the deletion of ZEB to miR-200 inhibitory link (*ZEB-miR200_2-0*) disrupted the mutually inhibitory loop between ZEB and miR-200. Similarly, converting the inhibitory link from ZEB to GRHL2 to being excitatory (*ZEB-GRHL2_2-1*) disrupted the mutually inhibitory feedback loop between ZEB and GRHL2 (**Fig 3A**). In the NRF2 network, converting the inhibitory link from ZEB to E-cadherin to being excitatory (*ZEB-Ecad_2-1*) disrupted the mutually inhibitory loop between ZEB and E-cadherin, and converting the inhibitory link from miR-200 to NRF2 to excitatory (*miR200-NRF2_2-1*) disrupted the overall positive feedback loop formed by miR-200, KEAP1, NRF2 and SNAIL (**Fig S2A**).

Previous analysis for simpler two-node networks has shown that mutually inhibitory and mutually excitatory loops (hence, both being overall positive loops) can lead to multistability which may drive phenotypic plasticity [34, 35]. Such networks are typically observed underlying the cell-fate decisions during embryonic development [36]. Similar observations have been made for miR-200/ZEB feedback loop in driving trans-differentiation through EMP [37, 38]. Therefore, we further inquired whether phenotypic plasticity can be correlated with the total number of positive feedback loops in a given network. We counted the number of positive feedback loops/cycles for all 'wild-type' and perturbed
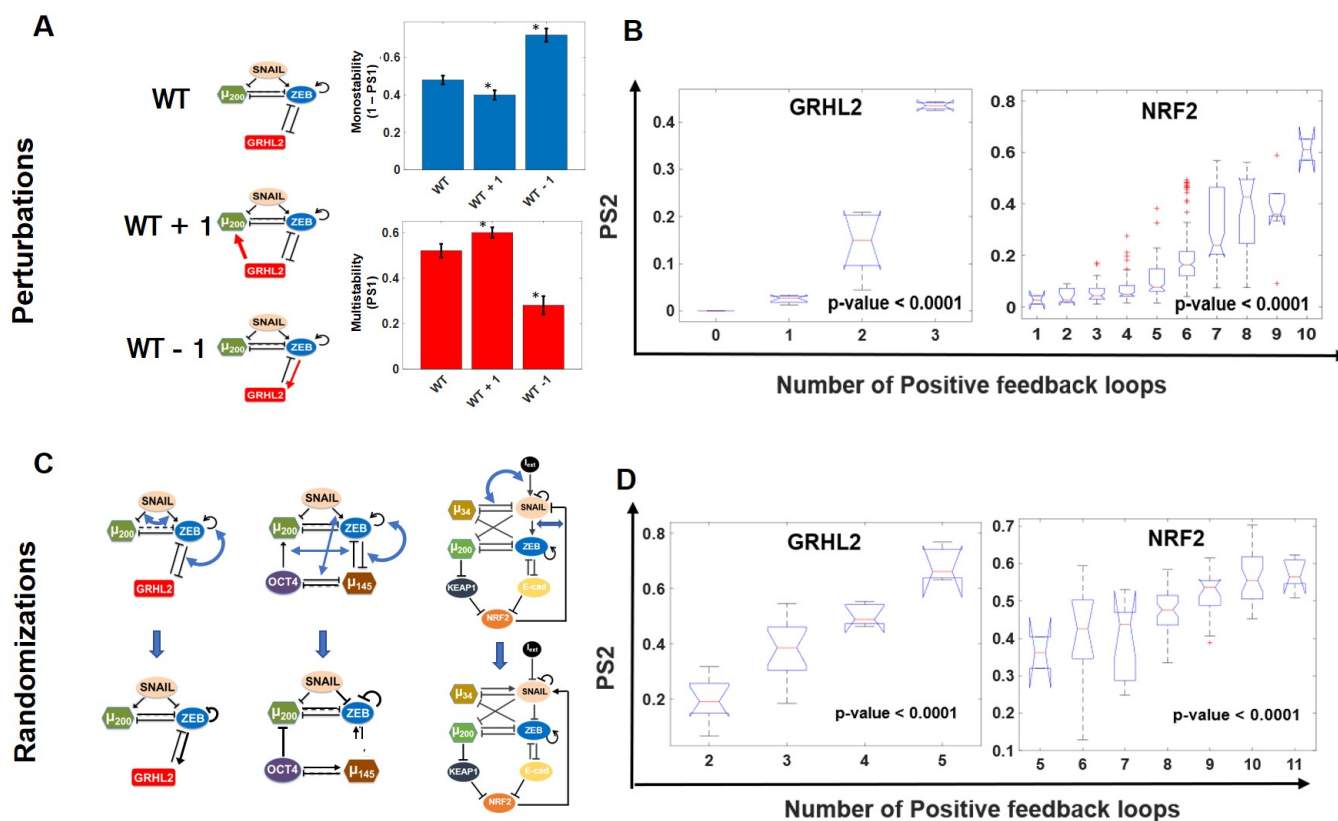
Figure 6: The number of positive feedback loops in EMP networks correlates with phenotypic plasticity A. Demonstration of change in plasticity on altering the total number of positive feedback loops in GRHL2 network. Frequency of multistable parameters (PS2) increases as compared to WT upon the addition of positive feedback loop (GRHL2-miR200-ZEB-GRHL2) to the network (WT + 1) and reduces upon reduction of positive feedback loops by changing the GRHL2-ZEB-GRHL2 cycle to negative feedback (WT − 1). B. Boxplots of PS2 vs. number of positive feedback loops for all the perturbed networks for a given EMP network module. One-way ANOVA test suggests a statistically significant positive correlation between positive feedback loops and plasticity. C. Demonstration of network randomization (the in-degree and out-degree of each node is preserved; however, the number of inhibitory/excitatory nodes arriving at or emerging from a node are not necessarily conserved). D. Same as B, but for randomized network topologies. One-way ANOVA suggests statistically significant positive correlation between positive feedback loops and plasticity. p-value range for the one-way ANOVA test are mentioned on the plots.

topologies for all six EMP networks (see Materials and Methods for description). First, taking GRHL2 network as a case study, we showed that decreasing the number of positive feedback loops by one (WT-1) reduced phenotypic plasticity (**Fig 6A**), while the reverse was true when the number of positive feedback loops was increased by one(WT + 1, **Fig 6A**).

Next, we compared the number of positive feedback loops in each perturbed network with the corresponding plasticity score. Box plots were used for comparison because the number of positive

13

feedback loops is a discrete quantity. Indeed, the mean plasticity score is higher for the groups of networks with higher number of positive feedback loops; this trend is observed across all six EMP networks in a statistically significant manner for both plasticity metrics – PS1, PS2 (**Fig 6B; S4A-B**), suggesting a correlation between the number of positive feedback loops in an EMP network, and its ability to give rise to phenotypic plasticity. We also observed that the total number of feedback loops (i.e., positive feedback loops + negative feedback loops) in the networks themselves did not exhibit any significant and consistent effect on plasticity, further emphasizing the role of positive feedback loops (**Fig S5**).

To test whether this observed correlation between plasticity scores and the number of positive feedback loops is specific to the network topology studied, we generated randomized topologies for each given network by swapping the edges in a given network (**Fig 6C**). This procedure preserves the in-degree and out-degree of each node in the network but can change the distribution of excitatory or inhibitory links arriving at (in-degree) or originating from (out-number) a given node. Thus, for a given EMP network, such randomization can generate various network topologies with varying number of net positive feedback loops. For each randomized network topology, we calculated PS1 and PS2. Similar to the perturbations, we observed a positive trend between plasticity and positive feedback loops (**Fig 6D; S4C-D**), strengthening our hypothesis that the number of positive feedback loops in a given EMP network is a good predictor of phenotypic plasticity.

Next, for all EMP networks, we calculated the JSD of the randomized networks from their 'wild-type' counterparts and plotted the corresponding plasticity scores on a two-dimensional plot of JSD from the 'wild-type' (x-axis) and the number of positive feedback loops (y-axis) for a given randomized topology (**Fig 7A, i; 7B,i**). As expected, there was heterogeneity in plasticity scores for a fixed number of positive feedback loops as well as for a fixed range of JSD, suggesting that plasticity scores might depend on both the number of positive feedback loops and JSD from the 'wild-type' network. Further analysis revealed that while the plasticity scores of the randomized topologies was significantly different for varied number of positive feedback loops (**Fig 6D; S4C-D**), no such significant difference was observed for varied range of JSD values (**Fig 7A, ii; 7B, ii**). This trend was seen across all six networks (**Fig S6**).

To further confirm our observations, we segregated the randomized topologies into cases with varied number of positive feedback cycles, and calculated correlation between plasticity scores and JSD from the 'wild-type' network. The correlation coefficient varied from -1 to 1, even within a given EMP network with many instances being statistically insignificant (**Fig 7C, i**). However,
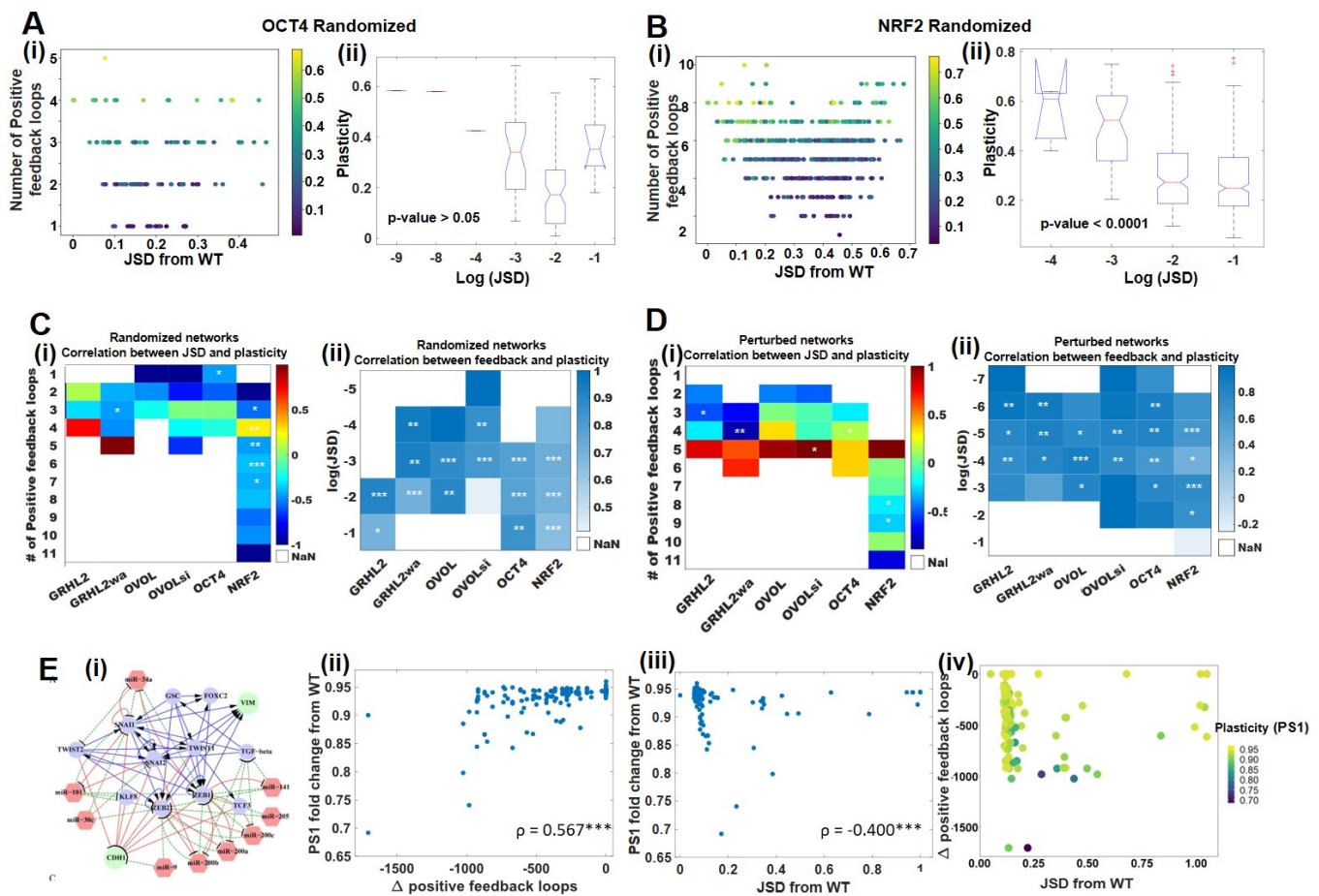
14

Figure 7: Correlation between JSD, plasticity, and number of positive feedback loops A. i) PS2 for every randomized network for OCT4 network module plotted as a function of its JSD from the WT network and number of positive feedback loops. Colorbar shows PS2 scores. ii) Boxplot for PS2 scores vs. range of JSD values for all networks plotted in i); no significant trend observed. p-value corresponds to one-way ANOVA test. B. Same as A but for NRF2 network C. i) For each EMP module, all randomized networks are sub-categorized based on number of positive feedback loops. Each cell denotes correlation coefficient between JSD from WT and plasticity score fold change, wherever applicable (i.e. number of samples corresponding to that network and feedback loop count > 3. The white boxes (NaN) represent the cases with number of samples less than 3). Spearman correlation coefficient shown using color bar; significance represented as : $*: p < 0.05, **: p < 0.01, ***: p < 0.001$ ii) For each EMP module, all randomized networks are classified based on range of JSD values. Each cell denotes correlation coefficient between plasticity score fold change and number of positive feedback loops. D. Same as C but for perturbed network for each EMP module. E. i) Larger EMP network with 22 nodes and 72 edges. ii) Scatter plot between PS1 fold change and a change in positive feedback loops of all perturbed networks (single-edge perturbations) corresponding to the larger EMP network. iii) Scatter plot of PS1 fold change from WT with JSD from WT for these networks. iv) Scatter plot of JSD from WT and change in positive feedback loops for each perturbed network. Color code denotes absolute value of PS1 for a given perturbed network topology.

when these randomized networks were segregated based on JSD, plasticity scores and number of positive feedback loops were positively correlated with statistical significance across all ranges of the JSD values and across the six EMP networks (**Fig 7C, ii**). Similar results were obtained for perturbed network topologies (i.e. the cases with perturbations – deletions and edge nature change and additions) across EMP networks (**Fig 7B; 7D**). Together, these results strongly support that the number of positive feedback loops, but not JSD, dictates phenotypic plasticity.

To examine the scalability of these results, we analysed a larger EMP network (**Fig 7E**, i; 22 nodes, 72 edges) and all single-edge deletions and edge nature change (activation to inhibition and vice-versa) perturbations (n=144) [25]. Given the network complexity, it becomes harder to associate mathematically observed stable steady states with biological phenotypes, and hence, we used the generic definition of phenotypic plasticity(PS1). The correlation between positive feedback loops and phenotypic plasticity was observed in this larger network as well (**Fig 7E, ii**). Interestingly, in this larger circuit, single-edge perturbations are capable of disrupting hundreds of positive feedback loops. The maximum number of positive loops disrupted by a single edge is approximately 1500; this perturbation can decrease the PS1 scores up to 30% (**Fig 7E; ii**). Given the large number of overall positive feedback loops in this network (n= 3111), the effect of disrupting a relatively small number of them does not have a pronounced effect on PS1 scores; however, we were able to identify single-edge perturbation that can halve the number of positive feedback loops in the network and correspondingly have a significant effect on phenotypic plasticity enabled by this network.

3. Discussion

Our ability to target phenotypic plasticity is limited by the understanding of its dynamics in tumors and the identification of tumor-specific molecular mechanisms driving it. While various transcriptional and epigenetic networks have been uncovered underlying phenotypic plasticity; how do these networks give rise to the co-existence of various drug-tolerant states, and the contribution of these different states to the minimal residual disease remain elusive [39]. Recent surge in our understanding of the dynamics of EMP has elucidated how the underlying EMP regulatory networks can give rise to various phenotypes/cell states along the spectrum of EMP, and how these different subpopulations may co-exist in a tumor and collaborate to drive tumor aggressiveness [40]. Nonetheless, targeting EMP in the clinic to observe a major reduction in metastasis still remains a challenge, because of the precise spatiotemporal regulation of EMP involved during metastasis. Thus, inhibiting one arm of EMP – say EMT – might actually promote MET and help colonization; and inhibiting

16

MET may facilitate more dissemin ation [7]. Moreover, inhibiting only EMT or MET may drive the cells into one or more hybrid E/M phenotypes that are considered to be the 'fittest' for metastasis [13]. Therefore, while targeting EMP is important for restricting metastasis and therapy resistance, how to achieve that remains an unsolved challenge.

Our results present a computational platform to identify specific inhibitors for EMP using a network-level approach. We have simulated various networks identified to underlie EMP using different modeling strategies, to dissect the design principles underlying those networks and suggest how perturbing those networks may prevent the ability of cells to switch back and forth among the E, M and hybrid E/M phenotypes. Our analysis predicts that reducing the total number of positive feedback loops in the EMP network can restrict plasticity. A recent experimental study offers preliminary validation of this prediction, where disrupting the miR-200/ZEB mutually inhibitory (hence, an overall positive feedback) loop via CRISPR led to significantly reduced metastasis in vivo [37]. This feedback loop has been identified as a key regulator of EMP through extensive experimental and computational analysis [27, 38, 41]. Mathematical modeling for this loop has predicted how clonal cells responding to the same EMT-inducing signal can display different phenotypes due to the emergent multistability (the co-existence of multiple steady states/ phenotypes), a prediction which was validated experimentally via single-cell analysis of EMP [37]. Various other EMP networks that have been mathematically studied have included various other direct or indirect positive feedback loops such as ZEB1/GRHL2 [28], ZEB1/ ESRP1 [42], ZEB1/miR-1199 [43], or miR-34/SNAIL [44].

Different modeling frameworks have been used to investigate the dynamics of EMP, depending on the size of network. While small-sized networks have typically been modelled via continuous approaches [45, 46, 9, 38, 47, 48], larger networks have been modelled via discrete Boolean approaches due to lack of available kinetic parameters [24, 43, 49, 50]. While continuous models provide a more quantitative mapping of system dynamics but require many kinetic parameters that can become experimentally intractable, Boolean modeling approaches provide a good estimate of qualitative behavior of a biochemical system without requiring a large set of parameters [51], but are limited in terms of characterizing dynamic properties such as phenotypic plasticity and state transition rates. Thus, various efforts have been made to compare the dynamics of Boolean vs. continuous models and to integrate their strengths, particularly for capturing steady state distributions for smaller biological networks [52, 53, 54].

Here, we compare the phenotypic distributions obtained for various EMP networks using Boolean approaches and using RACIPE [25] — an algorithm that generates an ensemble of continuous models,

17

each with a randomly chosen parameter set within a biologically feasible range. By simulating the models for a large number of parameter sets, this method tries to capture the parameteric variability observed in cell populations from one or multiple individuals. The qualitative and semi-quantitative agreement seen for Boolean and RACIPE models, across six EMP networks, enable us to understand the dynamics of EMP driven by network topology instead of specific kinetic parameter sets in a given cell/population. Furthermore, we could identify perturbations to the network topologies that affetced the phenotypic distributions significantly across parameter sets. Thus, our method to identify network-topology based predictions to inhibit EMP may provide an avenue to overcome a major bottleneck in targeted therapy — inter-individual variability in response. Moreover, through generating a larger number of randomized networks where the in-degree and out-degree of each node in the network was preserved, we showed that the phenotypic distributions and plasticity scores (PS1, PS2) obtained are specific to the particular topology of the networks regulating EMP. These results suggest evolutionary design principles of EMP networks that may have been optimized to induce EMP as/when needed during development/tissue regeneration, and stably maintain homeostatic differentiated phenotypes.

Intriguingly, the change in phenotypic plasticity, defined by both the plasticity scores does not correlate with JSD of phenotypic distributions. One possible reason underlying this perceivably confounding result can be that the JSD only computes the distance between two steady state distri-butions; it does not capture information about whether the phenotypes can switch among themselves. (Spontaneous) phenotypic switching is facilitated by multi-stable phases, i.e. the co-existence of more than one stable steady state, for a given parameter set. Our results that the number of positive feed-back loops in a given network determines the extent of phenotypic plasticity is reminiscent of reported connection between positive feedback loops and plasticity in other aspects of cancer too, where mu-tually inhibitory loops between two 'master regulators' drive phenotypic switching [55, 56, 57, 58]. Future efforts should aim at identifying which links(s) in the network to disrupt to cause maximal change in plasticity, because not every positive feedback loop may be equally likely to lead to mul-tistability [59, 60]. Moreover, for networks with the same number of feedback loops, the plasticity scores varied over a range, thus, identifying other predictors of plasticity based on network topology will be valuable. As an attempt to identify such complementary predictors, we investigated if JSD coupled with number of feedback loops can lead to isolate networks with highest plasticity, but no clear improvement in the trend was observed, eliminating JSD as a predictor of plasticity either individually or in combination with feedback loops.

349   Our results for the 26-node EMP network via RACIPE identifies an edge deletion that can reduce
350   the positive feedback loops to the half of its original value, and thus has a significant impact on the
351   plasticity. As more comprehensive networks representing the underlying biology are studied, RACIPE
352   becomes too computationally expensive, and hence network theory based measures to identify the
353   feedback loop that, when disrupted, can have maximal effect in curbing plasticity would be valuable
354   for future therapeutic applications.

355   Most of the targeted therapies in oncology target on disrupting a node in the network. Inevitably,
356   most cells identify 'escape' routes by navigating various dimensions of the phenotypic plasticity
357   landscape. Our results present an alternative and unorthodox mechanism to restrict the emergence
358   of metastasis and drug resistance – breaking the feedback loops, i.e. targeting a link instead of a node,
359   involved in phenotypic plasticity. Disrupting these feedback loops – the cornerstone of phenotypic
360   plasticity – can restrict the ability of cancer cells to adapt to various therapeutic attacks and limit
361   tumor aggressiveness.

4. Methods

4.1. RAndom CIrcuit PErturbaiton (RACIPE)

RACIPE [25] is a tool that simulates transcriptional regulatory networks (TRNs) in a continuous manner. Given a TRN, it constructs a system of ODE's representing the network, randomly samples parameters from pre-defined parameter ranges and simulates the models at each parameter set for multiple initial conditions, resulting an output of the collection of parameter sets and corresponding steady states obtained from the model. For the current analysis, we used a sample size of 10000 for parameter sets and 100 for initial conditions. The parameters were sampled via a uniform distribution and the ODE integration was carried out using Euler's method.

4.2. Boolean simulations

For discrete analysis of our networks, the Boolean algorithm devised by Font-Clos et al., [24] was used. The nodes are updated asynchronously according to a majority rule such that nodes state is set to 1 if the sum of activations to the node is more than the sum of inhibition and set to 0 if inhibition is more than activation. If inhibition and activations are equal, nodes are not updated. Steady state is said to have reached if the state of the network doesn't change over time-steps. The input for this formalism is a set of 10000 initial conditions, which are randomly sampled from all possible states of the system and corresponding steady states.

4.3. Discretization of RACIPE output and calculating the state frequency

For a given network with $i = [1, n]$ nodes, the steady state expression levels of the nodes were normalized in the following way:

$$E_{in} = \frac{E_i}{f_i}$$

$$f_i = \frac{g_i}{k_i} \prod_j \lambda_{ij}$$

Where, for the ith node, E_{in} is the normalized expression level, E_i is the steady state expression level, f_i is the normalization factor, g_i and k_i are production and degradation of the ith node corresponding to the current steady state and λ_{ij} are the fold change in expression of i due to node $j = [1, n]$. The normalized expression levels of all steady states are then converted into z-scores by scaling about their combined mean:

$$Z_i = \frac{E_{in} - \overline{E_{in}}}{\sigma_{in}}$$

where $\overline{E_{in}}$ is the combined mean and σ_{in} is the combined variance.

20

³⁸¹ The z-scores are then classified based on whether they are negative or positive into 0 (low) and 1

³⁸² (high) expression levels respectively. Each steady state of the network is thus labelled with a string

³⁸³ of 1's and 0's, discretizing the continuous steady state levels. We then calculate the total frequency

³⁸⁴ of each discrete state by counting the occurrence in all the parameter sets. For parameter sets with

³⁸⁵ n steady states, the count of each steady state is taken as 1/n, invoking the assumption that all the

³⁸⁶ states are equally stable.

³⁸⁷ *4.4. Quantitative convergence*

³⁸⁸ To estimate the optimal sample size of parameter sets for RACIPE and that of initial conditions

³⁸⁹ for Boolean models, all networks were simulated at different sample sizes in triplicates and the mean

³⁹⁰ an variance of the steady state frequency distribution was calculated. 10000 was estimated as the

³⁹¹ ideal sample sizes for both methods as it was the smallest sample size for which the variance in steady

³⁹² state frequencies was minimum and the mean of the same was consistently similar to that of higher

³⁹³ sample sizes.

³⁹⁴ *4.5. Jensen-Shannon Divergence to measure distance between phenotypic distributions*

To quantify the difference between two phenotypic distributions, an information theory metric, known as the Jensen-Shannon divergence (JSD) (Lin, 1991) was used, calculated for any two discrete frequency distributions $P(x) and Q(x)$ as:

$$JSD(P||Q) = \frac{1}{2}D(P||M) + \frac{1}{2}D(Q||M)$$

where $M = \frac{1}{2}(P + Q)$ and D denotes the Kullback-Leibler divergence, defined as

$$D(P||Q) = \sum_{x \in \varkappa} P(x) log(\frac{P(x)}{Q(x)})$$

³⁹⁵ The metric, JSD, varies between 0 and 1 when the base 2 logarithm is used for calculation, with 0

³⁹⁶ indicating identical distributions and 1 indicating no overlap between the two distributions.

³⁹⁷ *4.6. Calculating the number of positive feedback loops in a network*

³⁹⁸ We estimated the number of cycles in the networks using the *networkx* module in Python 3.7,

³⁹⁹ where a cycle is defined as a path traversed along the edges of a network that originates and ends at

⁴⁰⁰ the same node. We then combine the nature of edges in each cycle to determine whether the given

⁴⁰¹ cycle is positive or negative. For example, in the OCT4 network (Fig 1B), ZEB-miR200-ZEB is a

⁴⁰² positive feedback loop, as it goes through inhibition-inhibition. On the other hand, ZEB-miR145-

⁴⁰³ OCT4-miR200-ZEB is a negative feedback loop, as it goes through inhibition-inhibition-activation-

⁴⁰⁴ inhibition.

21

4.7. Statistical tests

All correlation analysis was done using Spearman correlation method using cor function in MAT-LAB. The corresponding statistical significance values are represented by '*'s, to be translated as: *: $p < 0.05$, **: $p < 0.01$, ***: $p < 0.001$. One-way ANOVA test was performed using anova1 function in MATLAB.

References

[1] Ben-Jacob E, Coffey DS, Levine H (2012) Bacterial survival strategies suggest rethinking cancer cooperativity. *Trends Microbiol.* 20(9):403–410.

[2] Celià-Terrassa T, Kang Y (2016) Distinctive properties of metastasis-initiating cells. *Genes Dev.* 30(8):892–908.

[3] Boumahdi S, de Sauvage FJ (2019) The great escape: tumour cell plasticity in resistance to targeted therapy. *Nat. Rev. Drug Discov.* doi : 10.1038/s41573-019-0044-1.

[4] Xue BK, Leibler S (2018) Benefits of phenotypic plasticity for population growth in varying environments. *Proc. Natl. Acad. Sci. U. S. A.* 115(50):12745–12750.

[5] Varga J, De Oliveira T, Greten FR (2014) The architect who never sleeps: Tumor-induced plasticity. *FEBS Lett.* 588(15):2422–2427.

[6] Lehúede C, Dupuy F, Rabinovitch R, Jones RG, Siegel PM (2016) Metabolic plasticity as a determinant of tumor growth and metastasis. *Cancer Res.* 76(18):5201–5208.

[7] Bhatia S, Monkman J, Toh AKL, Nagaraj SH, Thompson EW (2017) Targeting epithelial-mesenchymal plasticity in cancer: Clinical and preclinical advances in therapy and monitoring. *Biochem. J.* 474(19):3269–3306.

[8] Gupta PB, et al. (2011) Stochastic state transitions give rise to phenotypic equilibrium in populations of cancer cells. *Cell* 146(4):633–644.

[9] Jolly MK, et al. (2015) Coupling the modules of EMT and stemness: A tunable 'stemness window' model. *Oncotarget* 6(28):25161–25174.

[10] Fumagalli MR, Lionetti MC, Zapperi S, La Porta CAM (2019) Cross-Talk Between circRNAs and mRNAs Modulates MiRNA-mediated Circuits and Affects Melanoma Plasticity. *Cancer Microenviron.* doi : 10.1007/s12307-019-00230-4.

[11] Goldman A, et al. (2015) Temporally sequenced anticancer drugs overcome adaptive resistance by targeting a vulnerable chemotherapy-induced phenotypic transition. *Nat. Commun.* 6:6139.

[12] Gupta PB, Pastushenko I, Skibinski A, Blanpain C, Kuperwasser C (2019) Phenotypic Plasticity: Driver of Cancer Initiation, Progression, and Therapy Resistance. *Cell Stem Cell* 24(1):65–78.

23

[13] Jolly MK, Celià-Terrassa (2019) Dynamics of Phenotypic Heterogeneity during EMT and Stemness in Cancer Progression. *J. Clin. Med.* 8(10):1542.

[14] Nieto M Huang RY, Jackson RA, Thiery JP (2016) Emt: 2016. *Cell* 166(1):21–45.

[15] Dongre A, Weinberg RA (2019) New insights into the mechanisms of epithelial–mesenchymal transition and implications for cancer. *Nat. Rev. Mol. Cell Biol.* 20(2):69–84.

[16] Yuan S, Norgard RJ, Stanger BZ (2019) Cellular plasticity in cancer. *Cancer Discov.* 9(7):837–851.

[17] Jolly MK, Mani SA, Levine H (2018) Hybrid epithelial/mesenchymal phenotype(s): The 'fittest' for metastasis? *Biochimica et Biophysica Acta (BBA) - Reviews on Cancer* 1870(2):151–157.

[18] Tripathi S, Levine H, Jolly MK (2019) A Mechanism for Epithelial-Mesenchymal Heterogeneity in a Population of Cancer Cells. *bioRxiv* p. 592691.

[19] Salgia R, Kulkarni P (2018) The Genetic/Non-genetic Duality of Drug 'Resistance' in Cancer. *Trends in Cancer* 4(2):110–118.

[20] Neelakantan D, et al. (year?) EMT cells increase breast cancer metastasis via paracrine GLI activation in neighbouring tumour cells. *Nat. Commun.* 8:15773.

[21] Tsuji T, et al. (2008) Epithelial-mesenchymal transition induced by growth suppressor p12 CDK2-AP1 promotes tumor cell local invasion but suppresses distant colony growth. *Cancer Res.* 68(24):10377–10386.

[22] Williams ED, Gao D, Redfern A, Thompson EW (2019) Controversies around epithelial–mesenchymal plasticity in cancer metastasis. *Nat. Rev. Cancer* 19(12):716–732.

[23] Tripathi S, Xing J, Levine H, Jolly MK (2019) Mathematical Modeling of Plasticity and Heterogeneity in EMT. *arXiv Prepr.* arXiv:1907.11174.

[24] Font-Clos F, Zapperi S, La Porta CA (2018) Topography of epithelial–mesenchymal plasticity. *Proc. Natl. Acad. Sci. U. S. A.* 115(23):5902–5907.

[25] Huang B, et al. (2017) Interrogating the topological robustness of gene regulatory circuits by randomization. *PLoS Comput. Biol.* 13(3):e1005456.

[26] Gómez Tejeda Zañudo J, et al. (2019) Towards control of cellular decision-making networks in the epithelial-to-mesenchymal transition. *Phys. Biol.* 16(3):31002.

[27] Brabletz S, Brabletz T (2010) The ZEB/miR-200 feedback loop-a motor of cellular plasticity in development and cancer? *EMBO Rep.* 11(9):670–677.

[28] Mooney SM, et al. (2017) The GRHL2/ZEB Feedback Loop—A Key Axis in the Regulation of EMT in Breast Cancer. *J. Cell. Biochem.* 118(9):2559–2570.

[29] Jia D, et al. (2015) OVOL guides the epithelial-hybrid-mesenchymal transition. *Oncotarget* 6(17):15436–15448.

[30] Jolly MK, et al. (2016) Stability of the hybrid epithelial/mesenchymal phenotype. *Oncotarget* 7(19):27067–27084.

[31] Roca H, et al. (2013) Transcription Factors OVOL1 and OVOL2 Induce the Mesenchymal to Epithelial Transition in Human Cancer. *PLoS One* 8(10):e76773.

[32] Mehrazarin S, et al. (2015) The p63 gene is regulated by grainyhead-like 2 (GRHL2) through reciprocal feedback and determines the epithelial phenotype in human keratinocytes. *J. Biol. Chem.* 290(32):19999–20008.

[33] Nair M, Bilanchone V, Ortt K, Sinha S, Dai X (2007) Ovol1 represses its own transcription by competing with transcription activator c-myb and by recruiting histone deacetylase activity. *Nucleic Acids Research* 35(5):1687–1697.

[34] Chickarmane V, Troein C, Nuber UA, Sauro HM, Peterson C (2006) Transcriptional dynamics of the embryonic stem cell switch. *PLoS Comput. Biol.* 2(9):1080–1092.

[35] Gardner TS, Cantor CR, Collins JJ (2000) Construction of a genetic toggle switch in Escherichia coli. *Nature* 403(6767):339–342.

[36] Zhou JX, Huang S (2011) Understanding gene circuits at cell-fate branch points for rational cell reprogramming. *Trends Genet.* 27(2):55–62.

[37] Celià-Terrassa T, et al. (2018) Hysteresis control of epithelial-mesenchymal transition dynamics conveys a distinct program with enhanced metastatic ability. *Nat. Commun.* 9(1):5005.

[38] Lu M, Jolly MK, Levine H, Onuchic JN, Ben-Jacob E (2013) MicroRNA-based regulation of epithelial-hybrid-mesenchymal fate determination. *Proc. Natl. Acad. Sci. U. S. A.* 110(45):18144–18149.

[39] Rambow F, et al. (2018) Toward Minimal Residual Disease-Directed Therapy in Melanoma. *Cell* 174(4):843–855.e19.

[40] Jolly MK, et al. (2019) Hybrid epithelial/mesenchymal phenotypes promote metastasis and therapy resistance across carcinomas. *Pharmacol. Ther.* 194:161–184.

[41] Tian XJ, Zhang H, Xing J (2013) Coupled reversible and irreversible bistable switches underlying TGFβ-induced epithelial to mesenchymal transition. *Biophys. J.* 105(4):1079–1089.

[42] Jolly MK, et al. (2018) Interconnected feedback loops among ESRP1, HAS2, and CD44 regulate epithelial-mesenchymal plasticity in cancer. *APL Bioeng.* 2(3):031908.

[43] Silveira DA, Mombach JCM (2019) Dynamics of the feedback loops required for the phenotypic stabilization in the epithelial-mesenchymal transition. *FEBS J.* doi : 10.1111/febs.15062.

[44] Jia D, et al. (2017) Distinguishing mechanisms underlying EMT tristability. *Cancer Converg.* 1(1):2.

[45] Bocci F, et al. (2019) NRF2 activates a partial Epithelial-Mesenchymal Transition and is maximally present in a hybrid Epithelial/Mesenchymal phenotype. *Integr. Biol.* 11(6):251–263.

[46] Hong T, et al. (2015) An Ovol2-Zeb1 Mutual Inhibitory Circuit Governs Bidirectional and Multi-step Transition between Epithelial and Mesenchymal States. *PLoS Comput. Biol.* 11(11):e1004569.

[47] Huang B, et al. (2015) Modeling the transitions between collective and solitary migration phenotypes in cancer metastasis. *Scientific Reports* 5:17379.

[48] Kang X, Wang J, Li C (2019) Exposing the underlying relationship of cancer metastasis to metabolism and epithelial-mesenchymal transitions. *iScience* 21:754–772.

[49] Steinway SN, et al. (2014) Network modeling of TGFβ signaling in hepatocellular carcinoma epithelial-to-mesenchymal transition reveals joint sonic hedgehog and Wnt pathway activation. *Cancer Res.* 74(21):5963–5977.

26

[50] Steinway SN, et al. (2015) Combinatorial interventions inhibit TGFβ-driven epithelial-to-mesenchymal transition and support hybrid cellular phenotypes. *npj Syst. Biol. Appl.* 1:15014.

[51] Wynn ML, Consul N, Merajver SD, Schnell S (2012) Logic-based models in systems biology: A predictive and parameter-free network analysis method. *Integr. Biol.* 4(11):1332–1337.

[52] Saadatpour A, Albert R (2016) A comparative study of qualitative and quantitative dynamic models of biological regulatory networks. *EPJ Nonlinear Biomed. Phys.* 4(1):5.

[53] Samaga R, Klamt S (2013) Modeling approaches for qualitative and semi-quantitative analysis of cellular signaling networks. *Cell Commun. Signal.* 11(1):43.

[54] Wittmann DM, et al. (2009) Transforming Boolean models to continuous models: Methodology and application to T-cell receptor signaling. *BMC Syst. Biol.* 3(1):98.

[55] Huang B, et al. (2014) The three-way switch operation of Rac1/RhoA GTPase-based circuit controlling amoeboid-hybrid-mesenchymal transition. *Sci. Rep.* 4(1):6449.

[56] Jia D, Park J, Jung K, Levine H, Kaipparettu B (2018) Elucidating the Metabolic Plasticity of Cancer: Mitochondrial Reprogramming and Hybrid Metabolic States. *Cells* 7(3):21.

[57] Jolly MK, et al. (2014) Towards elucidating the connection between epithelial-mesenchymal transitions and stemness. *J. R. Soc. Interface* 11(101):20140962.

[58] Saha M, et al. (2018) AMPK–Akt double-negative feedback loop in breast cancer cells regulates their adaptation to matrix deprivation. *Cancer Res.* 78(6):1497–1510.

[59] Cherry JL, Adler FR (2000) How to make a biological switch. *J. Theor. Biol.* 203(2):117–133.

[60] Tiwari A, Igoshin OA (2012) Coupling between feedback loops in autoregulatory networks affects bistability range, open-loop gain and switching times. *Phys. Biol.* 9(5):55003.
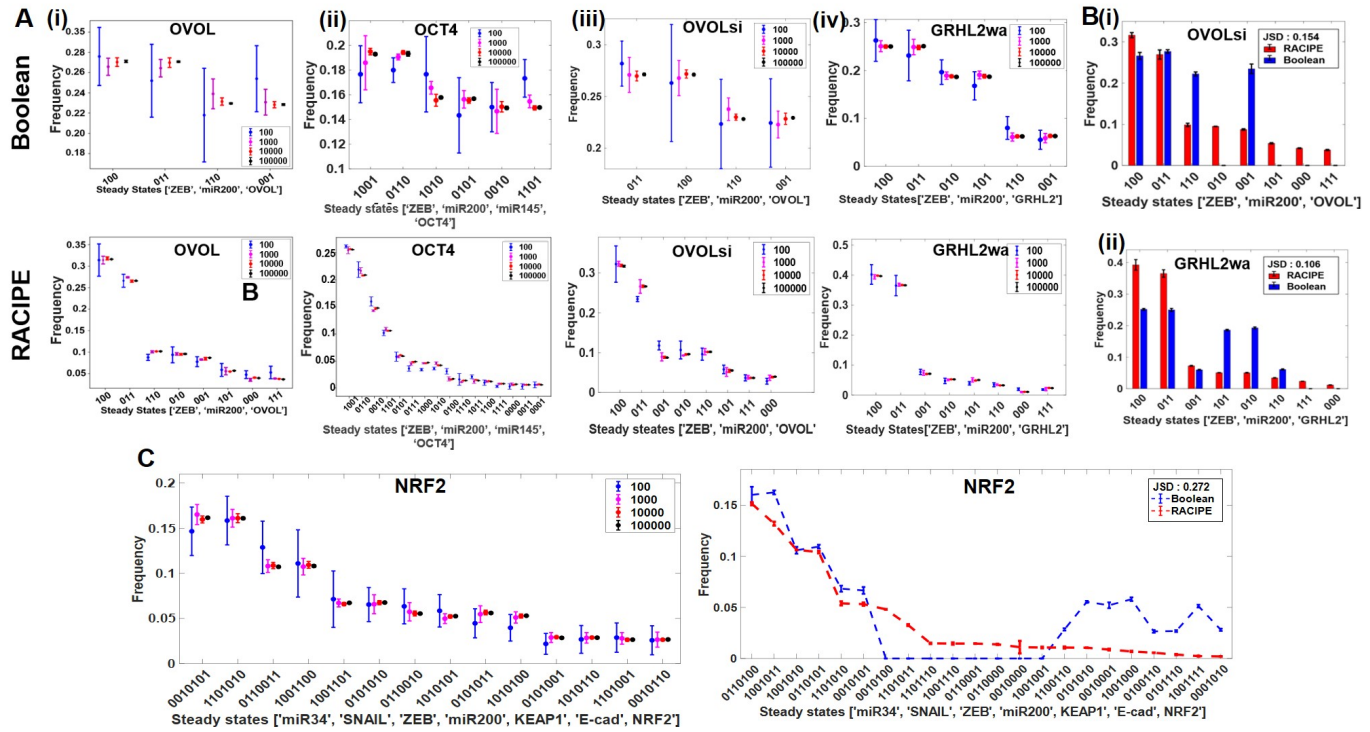
Supplementary Information

Figure S1: Quantitative convergence (QC) and comparison of phenotypic distributions obtained from RACIPE and Boolean A. QC of (i) OVOL, (ii) OCT4, (iii) OVOLsi and (iv) GRHL2wa using Boolean (top) and RACIPE (bottom). B. Comparision of steady state frequencies obtained from RACIPE and Boolean for GRHL2wa and OVOLsi C. NRF2 QC plot (Boolean) and comparison of RACIPE and Boolean state frequency distributions
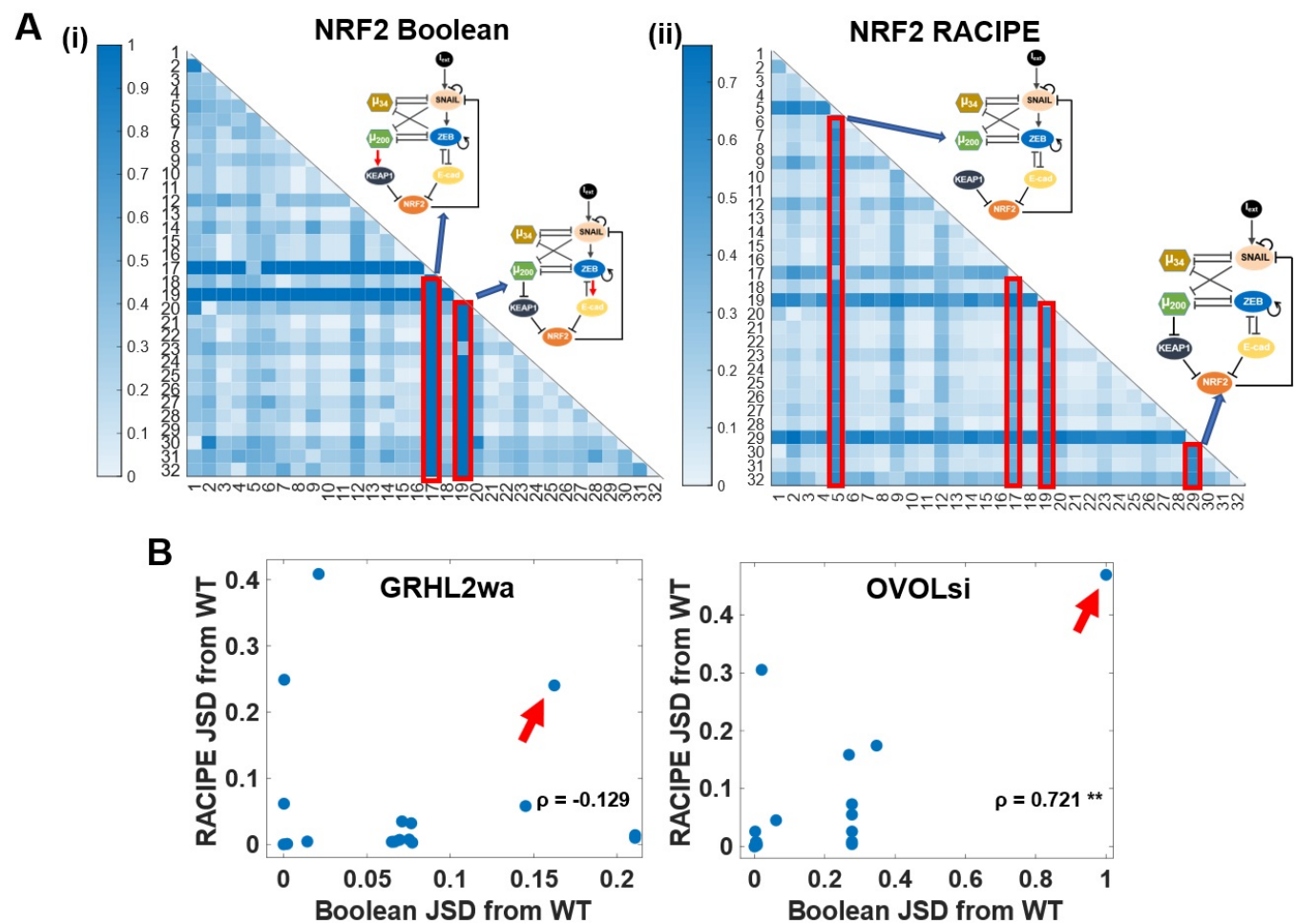
537

Figure S2: Effect of perturbations on phenotype distribution A. Heatmap of JSD of perturbations made to NRF2 network from each other (no edge additions) as obtained from i) Boolean and ii) RACIPE. Network 10 is 'wild-type'. The strongest perturbations are highlighted and the corresponding networks are shown with the heatmap. B. Scatter plots of JSD of perturbed networks from WT obtained from Boolean and RACIPE for GRHL2wa and OVOLsi.
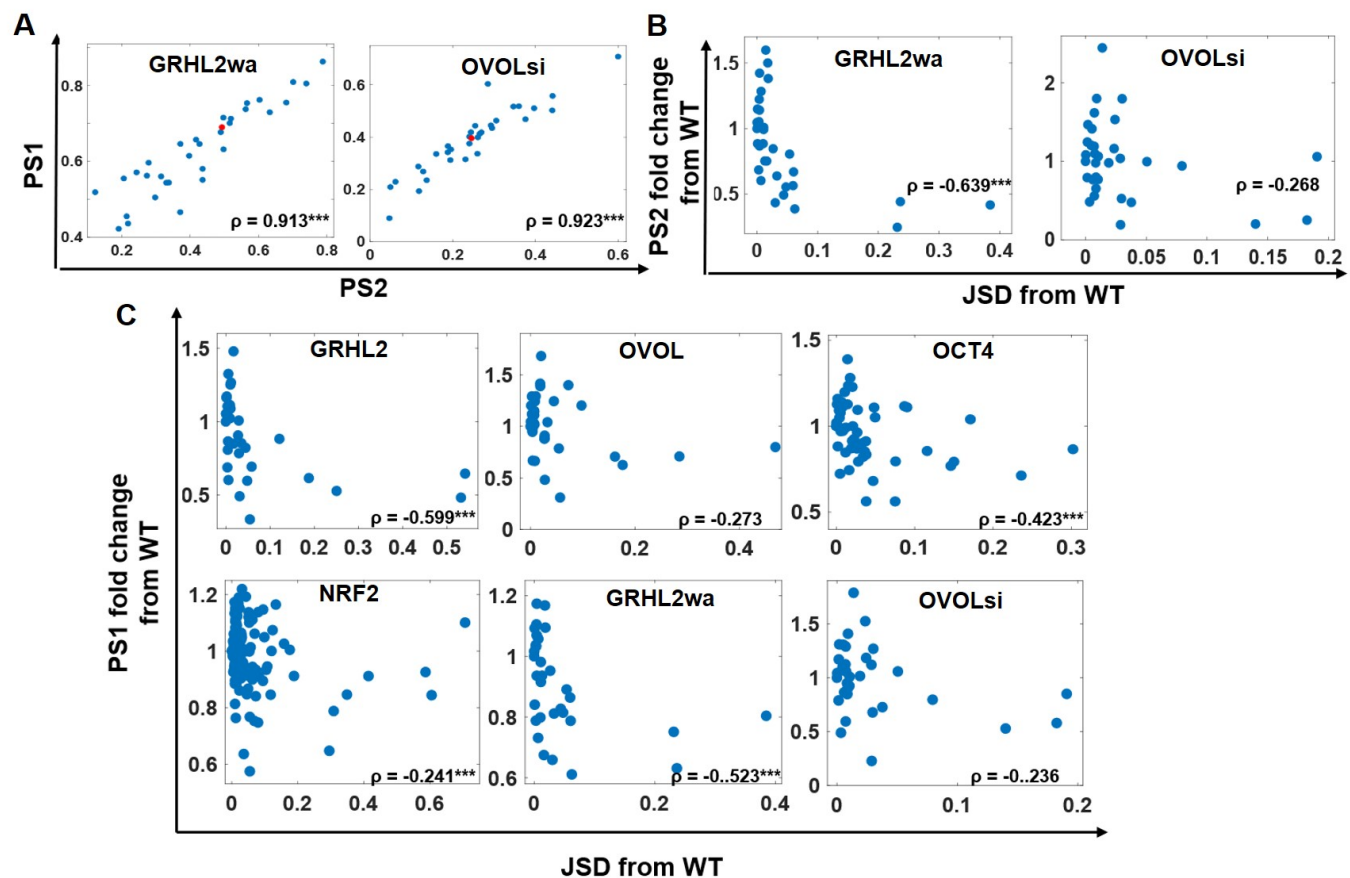
Figure S3: Effect of JSD on phenotypic plasticity A. Scatter plot between PS1 and PS2 for GRHL2wa and OVOLsi. B. Scatter plots for GRHL2wa and OVOLsi between fold change in plasticity vs change in phenotypic distribution (JSD). Each dot represents a perturbed network topology of the mentioned network. C. Same plots as B for all the networks, using PS1 instead of PS2
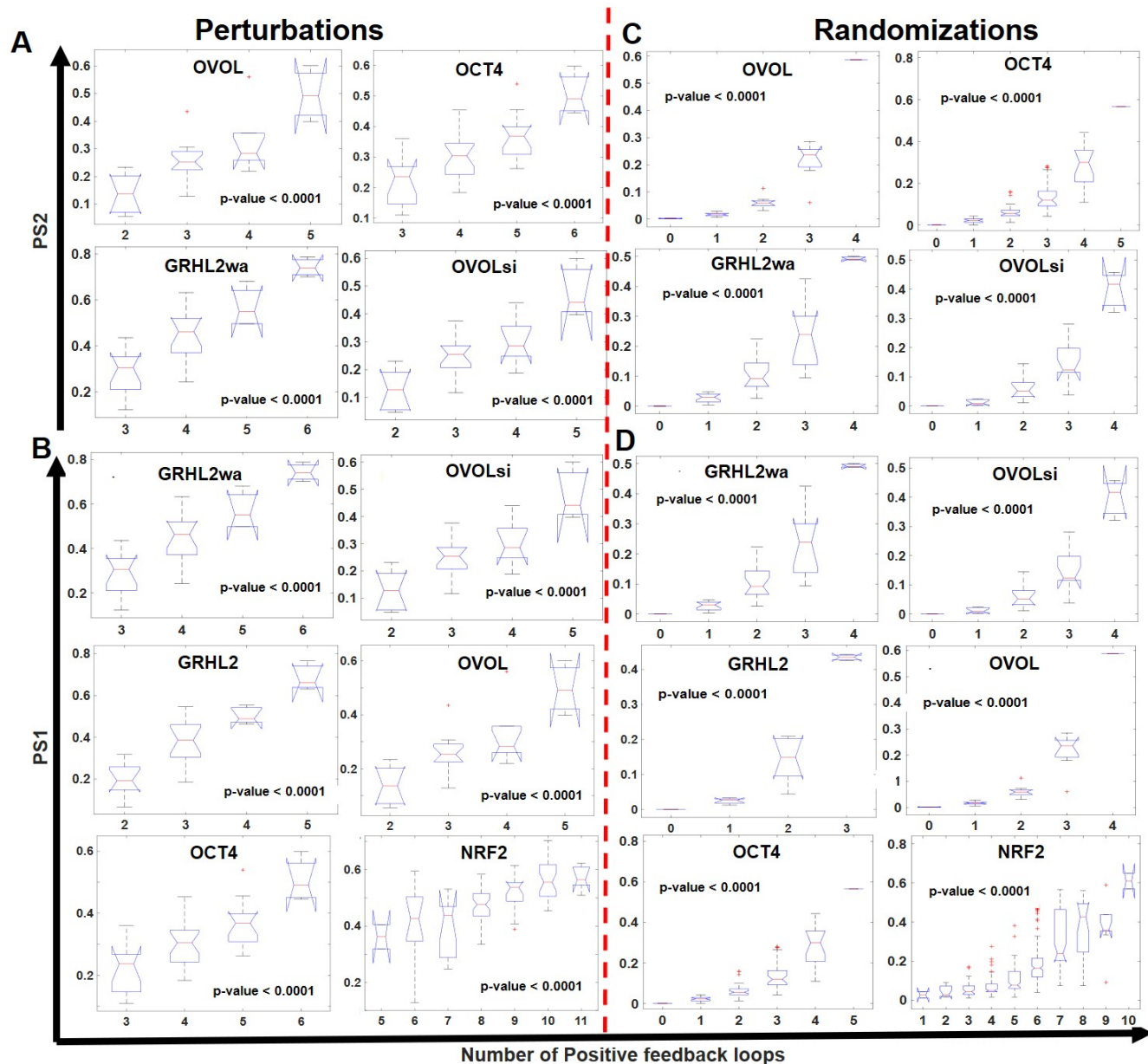
Figure S4: Effect of positive feedback loops on plasticity A. Box-plot of PS2 vs positive cycles for GRHL2wa and OVOLsi perturbed network topologies B. Box-plots of PS1 vs positive cycles for all perturbed network topologies coresponding to each EMP network C. Same as A but randomized circuits D. Same as B but randomized circuits
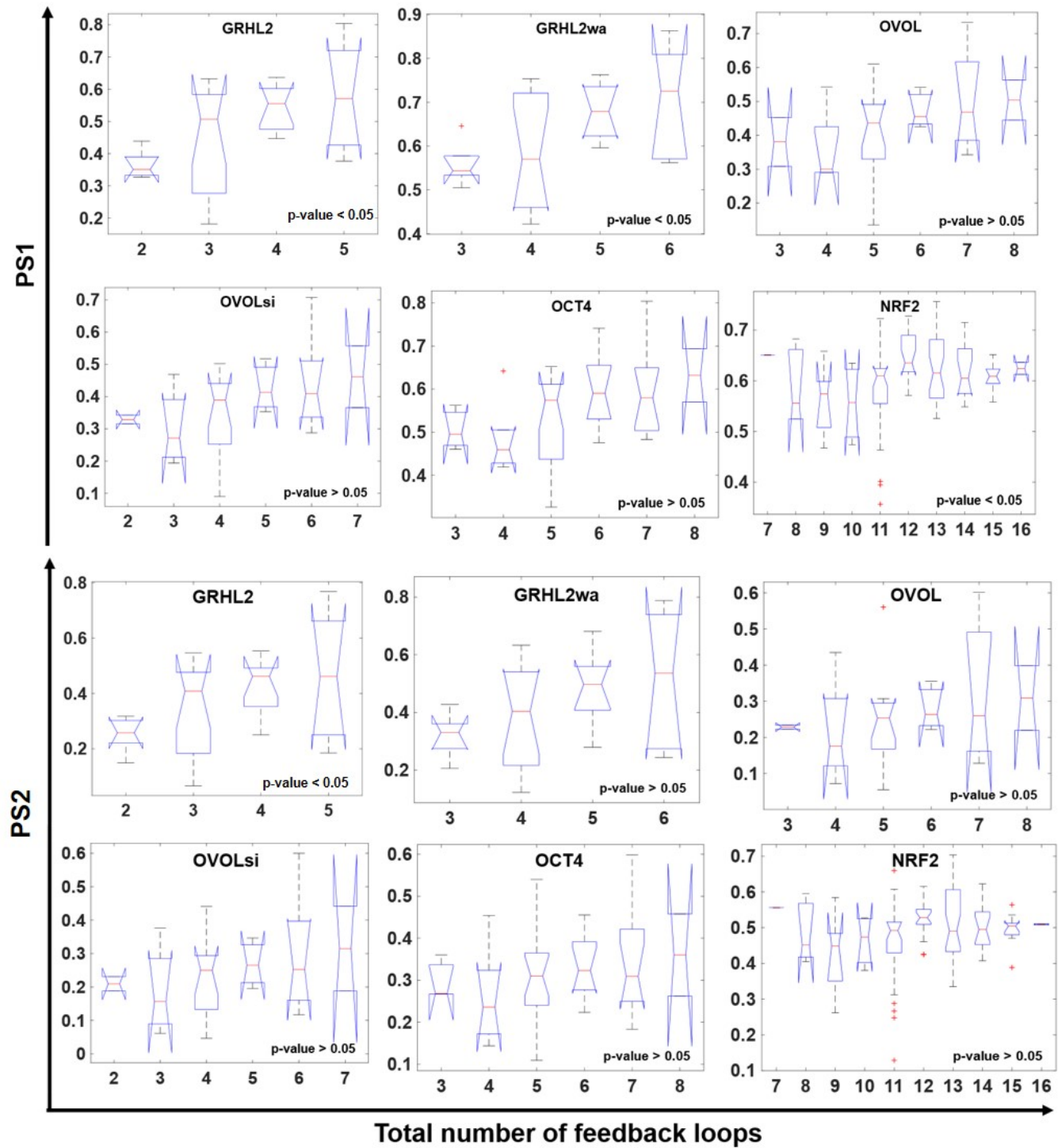
Figure S5: Effect of total number of feedback loops on network plasticity for perturbations of all 6 networks.
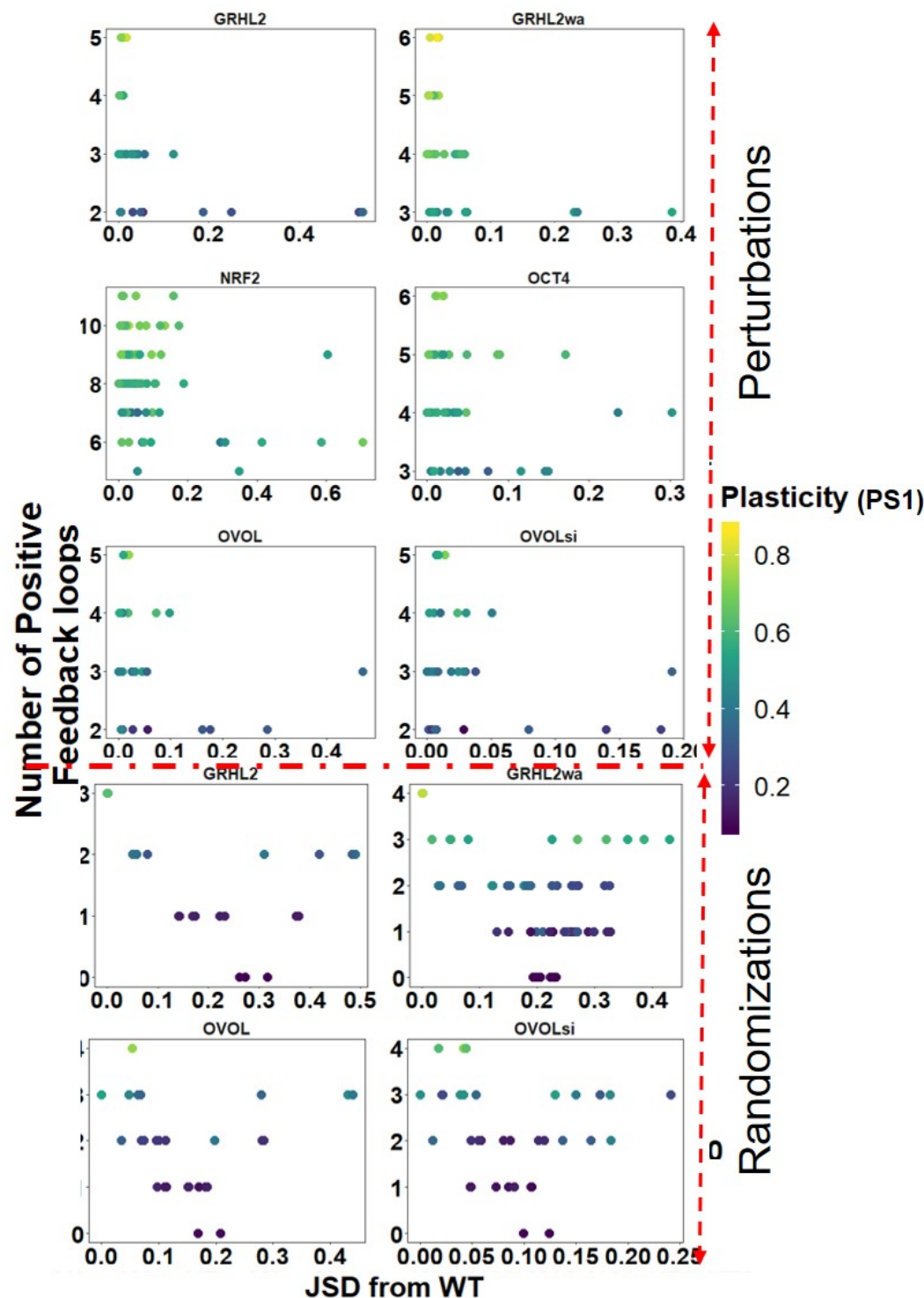
Figure S6: Combined effect of positive cycles and JSD on plasticity A. Positive cycles vs JSD scatter plots for perturbed network topologies of all 6 networks, colored according to plasticity B. Same as A but for randomized circuits

Table S1: GRHL2 single-edge perturbations including edge-additions. A given single edge perturbation is named as : FromNode-ToNode_OriginalEdge-PerturbedEdge. 0 : no edge, 1: activation, 2: inhibition

Label	Network
1	GRHL2-GRHL2_0-1
3	ZEB-miR200_2-1
4	GRHL2-GRHL2_0-2
5	miR200-miR200_0-1
6	miR200-ZEB_2-0
7	miR200-ZEB_2-1
8	SNAIL-SNAIL_0-1
9	ZEB-miR200_2-0
10	ZEB-ZEB_1-0
11	ZEB-ZEB_1-2
12	ZEB-GRHL2_2-0
13	ZEB-GRHL2_2-1
14	SNAIL-GRHL2_0-1
15	SNAIL-GRHL2_0-2
16	GRHL2-ZEB_2-0
17	GRHL2-ZEB_2-1
18	SNAIL-ZEB_1-2
19	GRHL2-miR200_0-1
20	GRHL2-SNAIL_0-2
21	GRHL2-miR200_0-2
22	GRHL2-SNAIL_0-1
23	SNAIL-ZEB_0-1
24	miR200-GRHL2_0-1
25	SNAIL-ZEB_0-2
26	SNAIL-ZEB_1-0
27	miR200-GRHL2_0-2
28	miR200-miR200_0-2
29	miR200-SNAIL_0-1
30	miR200-SNAIL_0-2
31	SNAIL-miR200_2-0
32	SNAIL-miR200_2-1

Table S2: NRF2 perturbations without edge-additions. A given single edge perturbation is named as : FromNode-ToNode_PreviousEdge-OriginalEdge. 0 : no edge, 1: activation, 2: inhibition

Label	Network
1	Keapl-NRF2_2-0
2	E-cad-NRF2_2-1
3	ZEB-ZEB_1-2
4	ZEB-miR34_2-0
5	miR200-Keap1_2-0
6	ZEB-miR200_2-0
7	SNAIL-miR34_2-0
8	SNAIL-ZEB_1-2
9	miR34-SNAIL_2-0
10	SNAIL-SNAIL_2-0
12	ZEB-miR200_2-1
13	miR200-ZEB_2-1
14	NRF2-SNAIL_2-1
15	E-cad-ZEB_2-1
16	ZEB-ZEB_1-0
17	miR200-Keapl_2-1
18	SNAIL-miR34_2-1
19	ZEB-E-cad_2-1
20	E-cad-NRF2_2-0
21	I-SNAIL_1-2
22	E-cad-ZEB_2-0
23	ZEB-E-cad_2-0
24	miR200-ZEB_2-0
25	SNAIL-miR200_2-0
26	SNAIL-SNAIL_2-1
27	SNAIL-miR200_2-1
28	NRF2-SNAIL_2-0
29	SNAIL-ZEB_1-0
30	Keapl-NRF2_2-1
31	miR34-SNAIL_2-1
32	ZEB-miR34_2-1